Carrier-mediated cavity optomechanics in a semiconductor laser

Xiang Xi, Jingwen Ma, and Xiankai Sun*
Department of Electronic Engineering, The Chinese University of Hong Kong, Shatin, New Territories, Hong Kong

(Received 17 July 2018; revised manuscript received 23 July 2018; published 23 May 2019)

Coherent interaction between photons and phonons plays a central role in cavity optomechanics. Additional physical degrees of freedom, such as electrons or atoms, can control the optomechanical interaction and thus serve as a coherent link between photons and phonons. Here, we study cavity optomechanics in a semiconductor gain medium where the inverted carriers interact collectively with the photons and phonons via the carrier relaxation oscillation and optical gain effects. With carrier relaxation oscillation, the carriers are coupled coherently to the mechanical modes via the optical field, which can be used to manipulate the phonon state. With optical gain effect, the inverted carrier population can tune the interaction between photons and phonons, rendering an enhancement of optomechanically induced slow light effect and a transition from optomechanically induced transparency to optomechanically induced absorption. The semiconductor-laser-based optomechanical systems offer substantial flexibility in coherent control of the photons and phonons, which may find wide applications in quantum metrology, information processing, and semiconductor laser engineering.

DOI: 10.1103/PhysRevA.99.053837

I. INTRODUCTION

Cavity optomechanics studies the coherent interaction between localized optical resonant modes and mechanical oscillation of a cavity [1,2], which may shed light on the transition from classical to quantum physics. Such interactions have been exploited for detecting and manipulating mechanical oscillation, resulting in unprecedented precision in displacement sensing [3] and optical cooling or heating of mechanical modes [4–7]. The optomechanical interaction is also harnessed for controlling light field, such as generating squeezed light [8,9] and demonstrating optomechanically induced transparency (OMIT) [10], which have promising applications in quantum metrology and signal processing. Therefore, exploration of coherent interaction among optics, mechanics, and other physical degrees of freedom has become an attractive topic for both quantum physics and technological applications [11–14]. Such hybrid optomechanical systems have been studied in a variety of media, e.g., piezoelectric materials [15,16], atom assembles [17–23], semiconductor materials [24,25], and Bose-Einstein condensates [26], leading to many interesting phenomena including regenerative mechanical oscillation [25], enhanced mechanical cooling [18,20,27], quantum entanglement [17,28], as well as tunable optical delay [10,16,21,29,30]. It is well known that in an optomechanical system, the optical transmission of a probe light field can be modified due to its interference with the mechanically scattered sideband of a control light field, which phenomenon is referred to as "optomechanically induced transparency (OMIT)" [10,16,29–31]. A typical feature is the drastic change of group velocity of the probe light passing through the system, producing slow or fast light [16,29] that can be used for photonic memories or signal processors.

Atomic ensembles have been extensively explored in optomechanics as a new degree of freedom to manipulate optomechanical coupling. It was discovered that radiation pressure control and mechanical entanglement can be achieved with the aid of atoms [17], which have been harnessed for enhancing phonon heating or cooling with substantial flexibilities [20,27,32–37]. The phenomena of OMIT and optomechanically induced absorption (OMIA) assisted by an atomic ensemble were studied previously. The effect of enhancement of radiation pressure and broadening of the OMIT window were discussed in Ref. [38]. The atom-photon coupling effects on OMIT were investigated in Ref. [39]. The auxiliary tunable slow or fast light by adjusting the atomic detuning and atom-photon coupling was discussed in Refs. [21,40]. In addition to the above studies, other physical degrees of freedom were also explored in the atom-involved systems. A degenerate optical parametric amplifier was included in an atom optomechanical system to control the properties of OMIA [41]. Another system was studied where the atoms are coupled directly with the mechanical modes rather than the optical modes [30]. Despite the interesting physics and versatile control in the optomechanical systems coupled with an atom ensemble, realization of these systems requires free-space cavities which allow for optical interaction with the atoms inside. To facilitate device miniaturization and system integration, we propose an on-chip implementation of a cavity optomechanical system, where the cavity is constructed in a semiconductor gain medium and the inverted carriers as the additional degree of freedom mediate the optomechanical coupling with more flexibilities than traditional atom ensembles.

Here, we study cavity optomechanics in a semiconductor gain medium where photons, phonons, and inverted carriers interact with each other. In a semiconductor laser, the

*xksun@cuhk.edu.hk

lasing optical modes exhibit damped relaxation dynamics due to fluctuations in carrier or photon population [42]. Such relaxation oscillation modes can induce a modulation to the radiation pressure on the mechanical oscillator, thus allowing the carriers to affect the mechanical modes. In turn, the mechanical oscillator can also influence the carriers as its motion generates Stokes and anti-Stokes sidebands of the lasing field. The interference between the relaxation oscillation mode and the mechanically scattered sideband of the lasing field modifies the built-in intracavity field, such that the output field carries the dynamic information of both the carriers' relaxation oscillation and mechanical vibration. Another important role of carriers is that they provide gain to the optical fields. In an OMIT system, the optical intensity and delay time depend largely on the cavity optical loss [10,16]. With smaller optical loss and lower thermal excitation from the gain medium [20], it is easier to obtain the OMIT phenomenon with enhanced slow or fast light effect. Besides, as the carrier relaxation oscillation and optical gain are associated with the laser steady-state photon and carrier number, the coupling among carriers, optical field, and mechanical modes can be tuned by the pumping strength [42].

This paper is structured as follows: Section II presents the theoretical model and equations of the system in which carriers, optical fields, and mechanical modes are involved. Section III analyzes coherent coupling of optical modes with mechanical mode and carrier relaxation oscillation in a semiconductor laser optomechanical system. Section IV shows that carrier-inversion-induced loss compensation can enhance the slow light effect and result in the phenomenon of optomechanically induced transparency or absorption that is largely tunable by the inverted carrier population. Section V concludes this paper.

II. THEORETICAL MODEL

We study a hybrid optomechanical system shown in Fig. 1(a), which consists of a typical cavity optomechanical system in a semiconductor gain medium [1]. The gain medium is pumped by an external electrical or optical source to generate inverted carriers, with inverted carrier number $\hat{N}$. These inverted carriers are coupled to the cavity optical field with amplitude $\hat{a}$ and frequency ω_L, which process can be modeled as a collective identical two-level system coupled to an optical field [27,43] with the Jaynes-Cummings Hamiltonian. Different from the hybrid atom optomechanical systems [21,30] which consider only a single two-level system, here we must consider the collective dynamics of carriers because of their large number in the semiconductor gain medium. Meanwhile, the optical field is also dispersively coupled to a mechanical oscillator, which vibrates at mechanical frequency Ω_m with displacement $\hat{x}(t)$ and effective mass $m_{\rm eff}$. We introduce a seeding signal with strength P_s and frequency ω_L into such an active optomechanical system so that it will also lase at the frequency ω_L under the external pump.

The Hamiltonian of the system is

$$\hat{H} = \hat{H}_{O\text{-}M} + \hat{H}_{A\text{-}O} + \hat{H}_s + \hat{H}_p, \tag{1a}$$

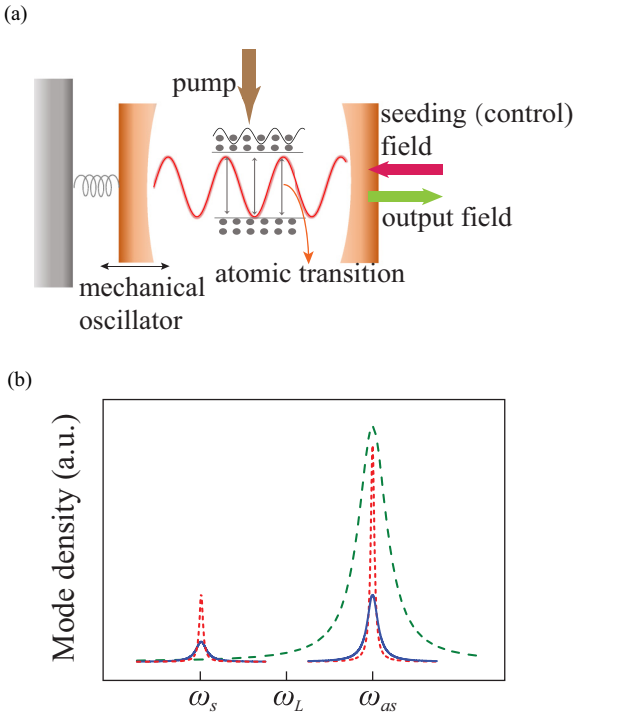

FIG. 1. (a) Illustration of an active cavity optomechanical system with gain material inside the cavity, where the population-inverted carriers interact with the optical field. (b) Optical sidebands in a passive cavity optomechanical system. The green dashed line delineates the transmission profile near the cavity resonant frequency $\omega_{\rm cav}$. An input optical mode at frequency ω_L is scattered by the mechanical mode to the Stokes ω_s and anti-Stokes ω_{as} components (red short-dashed lines). Additional modes (blue solid lines) emerge that originate from the carrier relaxation oscillation, which can have coherent interaction with the mechanical modes because they are both coupled to the intracavity optical field coherently.

with

$$\hat{H}_{O\text{-}M} = -\hbar\Delta_{L\text{-cav}}\hat{a}^\dagger\hat{a} + \hbar\Omega_m\hat{b}^\dagger\hat{b} - \hbar G x_{\rm ZPF}(\hat{b}^\dagger + \hat{b})\hat{a}^\dagger\hat{a}, \tag{1b}$$

$$\hat{H}_{A\text{-}O} = \frac{1}{2}\hbar\Delta_{L\text{-}a}\sum_k \hat{\sigma}_z^k + \hbar\mu_p\sum_k(\hat{a}^\dagger\hat{\sigma}_-^k + \hat{a}\hat{\sigma}_+^k), \tag{1c}$$

$$\hat{H}_s = P_s(\hat{a}^\dagger + \hat{a}). \tag{1d}$$

Here, $\hat{H}_{O\text{-}M}$ describes the dispersive optomechanical coupling in a cavity optomechanical system. The first two terms in Eq. (1b) are the Hamiltonian of the cavity optical field and mechanical mode. The photon annihilation (creation) operator is $\hat{a}$ ($\hat{a}^\dagger$) and the phonon annihilation (creation) operator is $\hat{b}$ ($\hat{b}^\dagger$). $\Delta_{L\text{-cav}} = \omega_L - \omega_{\rm cav}$ is the laser frequency detuning from the cavity resonant frequency $\omega_{\rm cav}$. The third term in Eq. (1b) describes the dispersive coupling between photons and phonons, where $G = -\partial\omega_{\rm cav}/\partial x$ is the cavity resonance shift per unit mechanical displacement [1] and $x_{\rm ZPF} = (\hbar/2m_{\rm eff}\Omega_m)^{1/2}$ is the zero-point fluctuation of the mechanical oscillator. $\hat{H}_{A\text{-}O}$ describes the interaction between the carriers and the optical field. The first term in Eq. (1c) denotes the energy of the active medium. $\Delta_{L\text{-}a} = \omega_L - \omega_a$

is the laser frequency detuning from the atomic transition frequency ω_a. The macroscopic population inversion between the two energy levels is represented by a sum of the Pauli operators, $\hat{N} = \sum_k \hat{\sigma}_z^k$, where the superscript k indicates each two-level system in the medium. The second term describes the interaction between the optical field and the medium polarization with coupling strength μ_p. The macroscopic polarization operator $\hat{p}$ is defined as $\sum_k \hat{\sigma}_+^k$ whose expectation value is the macroscopic polarization. $\hat{H}_s$ denotes the seeding signal with strength P_s. $\hat{H}_p$ denotes the pump that supplies energy to the laser system, which determines the macroscopic population inversion $\hat{N} = \sum_k \hat{\sigma}_z^k$.

Including the dissipation and fluctuation terms, the corresponding Heisenberg-Langevin equations of the active optomechanical system are

$$\dot{\hat{a}} = \left(i\Delta_{L\text{-cav}} - \frac{\kappa}{2}\right)\hat{a} - i\mu_p\hat{p} + iG\hat{x}\hat{a} + \hat{F}_a, \tag{2a}$$

$$\dot{\hat{p}} = \left(i\Delta_{L\text{-}a} - \frac{1}{T_p}\right)\hat{p} + i\mu_p\hat{a}\hat{N} + \hat{F}_p, \tag{2b}$$

$$\dot{\hat{N}} = \frac{1}{T_N}(N_{\text{st}} - \hat{N}) + 2i\mu_p(\hat{a}^\dagger\hat{p} - \hat{p}^\dagger\hat{a}) + \hat{F}_N, \tag{2c}$$

$$m_{\text{eff}}\left(\ddot{\hat{x}} + \Gamma_m\dot{\hat{x}} + \Omega_m^2\hat{x}\right) = \hbar G\hat{a}^\dagger\hat{a} + \hat{F}_x. \tag{2d}$$

These equations are expressed in the rotating frame of the seeding (control) field's frequency ω_L. κ is the cavity's optical intensity decay rate which includes the contributions from extrinsic coupling (κ_{ex}) and intrinsic loss (κ_0). N_{st} denotes the inverted carrier population at equilibrium in the absence of cavity field, which is determined by the pump strength. T_p and T_N are the relaxation time of medium polarization and carrier population inversion, respectively. Γ_m is the damping rate of the mechanical oscillator. $\hat{x} = x_{\text{ZPF}}(\hat{b} + \hat{b}^\dagger)$ is the mechanical displacement. $\hat{F}_a$, $\hat{F}_p$, $\hat{F}_N$, and $\hat{F}_x$ are the quantum and thermal noise terms, which will be dropped in the subsequent analysis because their average values are zero [10,21,42]. Therefore, we can substitute the operator notation of the variables with their expectation values $\hat{y} \to y\,(y \equiv \langle\hat{y}\rangle)$, as our study remains in the classical regime. In what follows, we will discuss the roles of inverted carriers in semiconductor laser optomechanical systems.

III. OPTOMECHANICS WITH CARRIER RELAXATION OSCILLATION

In this section, we study the coherent coupling between a mechanical oscillator and inverted carriers by considering the carrier-relaxation-oscillation effect in an optomechanical cavity. The introduction of optical gain brings great flexibility for controlling the optomechanical coupling. In a typical single-mode laser, its power spectrum consists of a lasing mode with the Stokes and anti-Stokes sidebands offset at the system's relaxation oscillation frequency Ω_r [42]. These sidebands are produced by the carriers' relaxation oscillation from the carrier dynamics [44,45], similar to those produced by external harmonic modulation to the carriers or optical fields. The beating of the lasing mode (ω_L) and the relaxation oscillation sidebands ($\omega_L \pm \Omega_r$) can generate an optical force oscillating at frequency Ω_r. If Ω_r is near the mechanical oscillator's resonant frequency Ω_m, the mechanical mode can oscillate coherently with the carrier-relaxation-oscillation mode. Since the mechanical mode also scatters the lasing mode producing the Stokes and anti-Stokes sidebands, the coherent interaction between the mechanical mode and the carrier-relaxation-oscillation mode can be identified in the interference patterns in the Stokes and anti-Stokes sidebands.

The coherent coupling between light and mechanical oscillation can usually be identified by measuring an additional probe field sent into the optomechanical cavity [10]. However, this scheme is not applicable for investigating the role of the inverted carriers' relaxation effect in the semiconductor laser optomechanical system. If a weak probe field with frequency $\omega_p = \omega_L + \Omega$ is sent into the laser optomechanical cavity, the probe-field-induced relaxation sidebands are orders of magnitude weaker than the built-up probe field in the cavity. As a result, in this situation the carrier-relaxation-oscillation-induced optical sidebands play a negligible role in the intracavity field interference, and the output spectrum carries little information about the coupling between the mechanical modes and the carrier-relaxation-oscillation modes. To avoid strong buildup of the probe field in the cavity, the probe signal can be sent into the cavity by weakly modulating the laser pump with a rf frequency Ω, as shown in Fig. 2(a). This results in a modulation of the carrier population inversion, $\delta N_I = N_I\cos(\Omega t)$, which should be included in Eq. (2c) such that

$$\dot{N} = \frac{1}{T_N}(N_{\text{st}} - N) + 2i\mu_p(a^*p - p^*a) + \delta N_I. \tag{3}$$

The relaxation oscillation of carriers is usually produced by perturbations of the pump. When the carrier population inversion is above the threshold value, the system works in the lasing regime at the frequency ω_L locked by the seeding signal. The mechanical vibration and collective carrier oscillation can both modulate the intracavity optical field, generating sidebands of the lasing mode. Meanwhile, the optical field can also produce backaction on the carriers and mechanical modes. Therefore, coupling between the carrier relaxation oscillation and mechanical vibration is established.

Equations (2a)–(2d) are a set of coupled nonlinear equations, and thus multiple equilibrium states may exist, yielding optical bistability [46]. Here we are interested in the small-signal dynamics, so we focus on the sideband picture and linearize the operators in Eqs. (2a)–(2d). The solutions near the classical steady state of the system should take the following forms:

$$a(t) = \bar{a} + A^-e^{-i\Omega t} + A^+e^{i\Omega t}, \tag{4a}$$

$$x(t) = \bar{x} + Xe^{-i\Omega t} + X^*e^{i\Omega t}, \tag{4b}$$

$$p(t) = \bar{p} + P^-e^{-i\Omega t} + P^+e^{i\Omega t}, \tag{4c}$$

$$N(t) = \bar{N} + N_0e^{-i\Omega t} + N_0^*e^{i\Omega t}. \tag{4d}$$

The above equations are expressed in the rotating frame of ω_L, so the actual frequency of the small optical signal is $\omega_L \pm \Omega$. The steady-state values of the operators $\bar{a}$, $\bar{x}$, $\bar{p}$, and $\bar{N}$ are orders of magnitude larger than their respective small sideband signals $A^\pm$, X, X^*, $P^\pm$, N_0, and N_0^*. $\bar{a}$ and $\bar{N}$ depend on the pump strength as well as the threshold and saturation effect of the laser system [43]. The output spectral response to the pump fluctuation δN_I is defined as $A^- = \chi(\Omega)N_I$, where

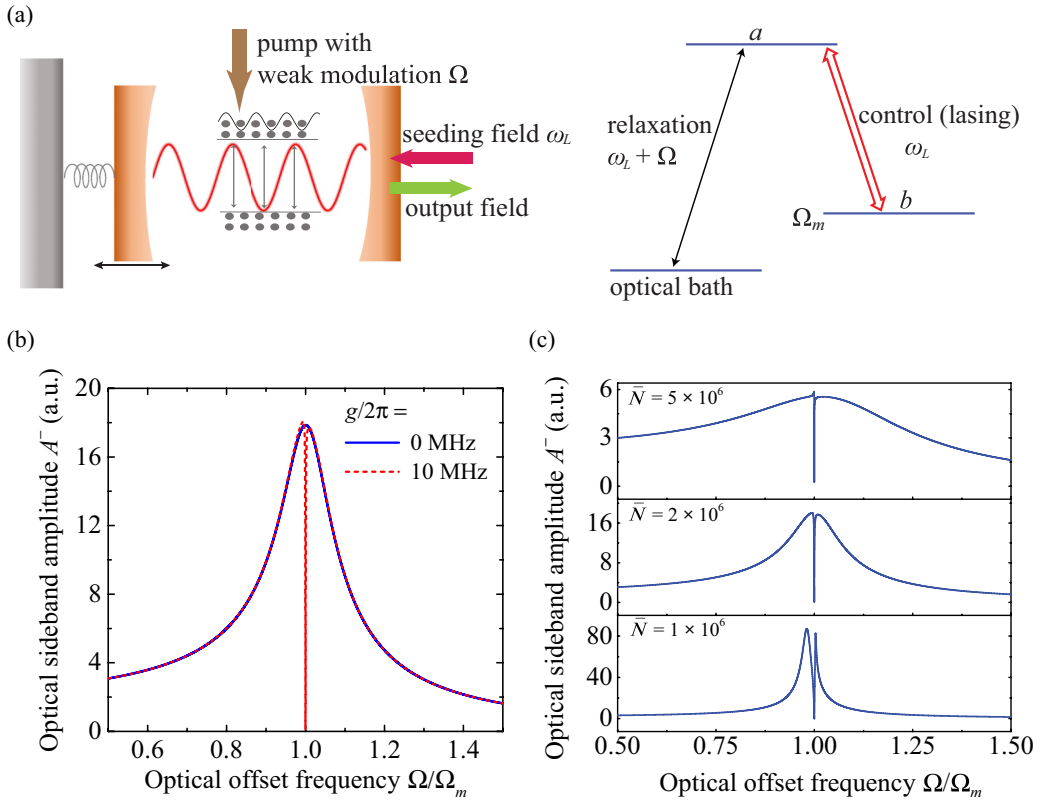

FIG. 2. (a) Left: Illustration of the interaction among the carriers, optical field, and mechanical mode. The carrier relaxation oscillation is actuated by a weak modulation to the pump. Right: Energy-level diagram showing the three energy levels of the optical mode a, the mechanical mode b, and the optical bath. The transition between the optical bath and the optical mode a is enabled by the system's relaxation oscillation, indicated by the black double-headed arrow. The transition between the mechanical mode b and the optical mode a is driven by the lasing mode, indicated by the red double-headed arrow. (b) Optical sideband amplitude produced by carrier relaxation oscillation without and with the mechanical mode, denoted by the blue solid line and red dashed line, respectively. (c) Optical sideband amplitude of the semiconductor laser optomechanical system with increasing population of inverted carriers. The parameters used for plotting (b) and (c) are $(\Delta_{L\text{-cav}}/2\pi, \Delta_{L\text{-}a}/2\pi, \kappa/2\pi, T_p, T_N, \bar{N}, \bar{n}, \mu_p/2\pi, m_{\text{eff}}, \Gamma_m/2\pi, \Omega_m/2\pi) = (-1.25\,\text{GHz}, 1\,\text{GHz}, 100\,\text{MHz}, 16\,\text{ps}, 1.6\,\text{ns}, 2\times10^6, 2.5\times10^6, 1\,\text{MHz}, 1\,\text{ng}, 2\times10^4\,\text{Hz}, 1.3\,\text{GHz})$ [27,43]. With these parameters, the relaxation oscillation frequency is ∼1.3 GHz and the optomechanical coupling rate is $g/2\pi = Gx_{\text{ZPF}}\bar{n}^{1/2}/2\pi = 10$ MHz.

$\chi(\Omega)$ is the susceptibility expressed as (see Appendix A)

$$\chi(\Omega) = \frac{\frac{\lambda(\Omega)\bar{a}[\varphi^*(-\Omega)+\varphi(\Omega)]}{f(\Omega)-f^*(-\Omega)} + \varphi(\Omega)\bar{a}}{\Omega_r^2 - \left(\Omega + \frac{\bar{\Delta}_{L\text{-cav}}}{2} + i\Gamma_r\right)^2 + (\Gamma_n - i\Omega)\lambda(\Omega)}, \quad (5a)$$

with

$$\lambda(\Omega) = \frac{i\hbar G^2\bar{n}[f(\Omega) - f^*(-\Omega)]}{f^*(-\Omega)\Psi_m(\Omega)}, \quad (5b)$$

$$\varphi(\Omega) = \frac{\mu_p^2}{-i(\Delta_{L\text{-}a} + \Omega) + 1/T_p}, \quad (5c)$$

$$f(\Omega) = -i(\bar{\Delta}_{L\text{-cav}} + \Omega) + \frac{\kappa}{2} - \varphi(\Omega)\bar{N}, \quad (5d)$$

$$\Omega_r^2 = \frac{[\varphi^*(-\Omega)f(\Omega) + f^*(-\Omega)\varphi(\Omega)]Q_0\bar{a}}{f^*(-\Omega)} - \frac{(\Gamma_n - \Gamma_p + i\bar{\Delta}_{L\text{-cav}})^2}{4}, \quad (5e)$$

$$\Psi_m(\Omega) = m_{\text{eff}}\left(-\Omega^2 - i\Gamma_m\Omega + \Omega_m^2\right), \quad (5f)$$

$$A_{21} = \frac{2\mu_p^2/T_N}{1/T_N^2 + \Delta_{L\text{-}a}^2}. \quad (5g)$$

In Eqs. (5a)–(5g), $\bar{\Delta}_{L\text{-cav}} = \Delta_{L\text{-cav}} - G\bar{x}$ is the effective laser frequency detuning. Ω_r is the relaxation oscillation frequency of the system. $\Gamma_n = 1/T_N + 2A_{21}\bar{n}$, $\Gamma_p = \kappa/2 - \varphi(\Omega)\bar{N}$, and $\Gamma_r = (\Gamma_n + \Gamma_p)/2$ denote the effective damping rates of the carriers, optical amplitude, and relaxation oscillation, respectively. $\bar{n} = |\bar{a}|^2$ is the average intracavity photon number. A_{21} is the stimulated emission rate. $Q_0 = 2A_{21}\bar{N}\bar{a}$ is the differential optical gain. The laser relaxation oscillation sidebands can be retrieved by disabling the mechanical interaction with a zero optomechanical coupling rate ($G = 0$) in the above equations. The light-enhanced optomechanical coupling rate in the linearized regime is $g = Gx_{\text{ZPF}}\bar{n}^{1/2}$.

The susceptibility $\chi(\Omega)$ in Eq. (5a) is asymmetric with respect to the rotating frequency ω_L because of the laser detuning from the cavity resonance. In the case of red-detuning, the mechanically induced Stokes mode and the carrier-relaxation-oscillation-induced lower sideband are strongly suppressed because they are distant from the cavity resonance. In Fig. 2(b), the blue solid and red dashed lines show the carrier-relaxation-induced optical sideband without and with

coupling to the mechanical mode, respectively. It is clear that the mechanical-mode-induced anti-Stokes sideband couples destructively to the carrier-relaxation-induced sideband, producing a dip centered at the mechanical frequency. The depth and width of the dip are determined by the optomechanical coupling strength, effective optical damping, and mechanical damping. Figure 2(c) plots the optical sideband due to coupling with both the carrier relaxation oscillation and mechanical vibration at different levels of carrier population inversion. In a semiconductor laser, larger inverted carrier population produces higher carrier-relaxation-oscillation frequency, and also increases the damping rates of the carriers and relaxation oscillation [42]. At $\bar{N} = 1 \times 10^6$, the carrier-relaxation-oscillation frequency is slightly below the mechanical frequency. The interaction of the two modes yields a sharp Fano resonance sitting on the right shoulder of the broad peak of the carrier relaxation resonance [Fig. 2(c), bottom]. At $\bar{N} = 2 \times 10^6$ or 5×10^6, the relaxation oscillation frequency becomes equal to or larger than the mechanical frequency, producing a Lorentzian dip at the top [Fig. 2(c), middle] or a Fano line shape on the left shoulder of the broad peak [Fig. 2(c), top], respectively. It should be noted that the relaxation oscillation mode originates from the pump modulation δN_I, so the appearance of strong Fano resonances indicates strong coupling between the phonons and the drive signal. Since the modulation drive signal can be applied through either optical pumping or electric current injection, we can obtain coherent coupling between rf or microwave signals and mechanical oscillations with a scheme that opens a way to manipulate and detect the mechanical motions.

IV. OPTOMECHANICS WITH CARRIER-INDUCED GAIN

Besides introducing the carrier relaxation oscillation, another important role of a semiconductor gain medium is that it can supply gain to the intracavity optical field. When the system operates below the lasing threshold, the supplied gain can reduce the optical loss experienced by the incident probe field. Above the lasing threshold, the supplied gain can amplify the probe field. The gain controlled by the inverted carrier population can thus change both the dispersion and phase of probe light passing through the cavity. In a passive optomechanical system, the cavity can exhibit transparency for the probe light through interference between the mechanically scattered sidebands and the probe light, which phenomenon is referred to as OMIT [10]. Within the transparency window, the probe field experiences an abrupt phase change, leading to slow or fast light. In this section, we study how the gain supplied to the optomechanical cavity affects the cavity transmission of probe light.

As shown in Fig. 3(a), a probe field E_p with frequency $\omega_p = \omega_L + \Omega$ is injected into an active optomechanical system. Its transmission can be solved from Eqs. (2a)–(2d) with Eq. (2a) modified as

$$\dot{a} = \left(i\Delta_{L\text{-cav}} - \frac{\kappa}{2}\right)a - i\mu_p p + iGxa + \sqrt{\eta_c\kappa}E_p e^{-i\omega t}, \quad (6)$$

where $\eta_c = \kappa_{\text{ex}}/\kappa$ and κ_{ex} is the in- or out-coupling-induced cavity decay rate [10]. Using the same ansatz as that in Eqs. (4a)–(4d), we can get the intracavity optical field of the probe light. Under the red-detuning condition, the optical sideband A^- is much stronger than the other sideband A^+ because A^+ is farther away from the cavity resonance. Therefore, we focus only on the optical sideband A^-. Using the standard input-output relation [10,16], we obtain the transmissivity for the probe signal E_p (see Appendix B),

$$\begin{aligned} T_{\text{probe}} &= \frac{E_p - \sqrt{\eta_c\kappa}A^-}{E_p} \\ &= 1 - \frac{\frac{\varphi^*(-\Omega)Q_0\bar{a}}{f^*(-\Omega)} + (\Gamma_n - i\Omega)\frac{f^*(-\Omega)\Psi_m(\Omega) + i\hbar G^2\bar{n}}{f^*(-\Omega)\Psi_m(\Omega)}}{\Omega_r^2 - \left(\Omega + \frac{\bar{\Delta}_{L\text{-cav}}}{2} + i\Gamma_r\right)^2 + (\Gamma_n - i\Omega)\lambda(\Omega)}\eta_c\kappa. \end{aligned} \quad (7)$$

The phase response is defined as $\Phi(\Omega) = \text{Arg}[T_{\text{probe}}(\Omega)]$ and the corresponding group delay is expressed as $\tau(\omega) = -d\Phi/d\Omega$ [10].

When carriers are not involved ($\bar{N} = 0$), the transmissivity T_{probe} reduces to that of a passive optomechanical system. When carrier population inversion is taken into account ($\bar{N} \neq 0$), the cavity field will interact with both carriers and mechanical modes simultaneously. Although the carrier-relaxation-oscillation-induced optical sidebands play a negligible role in the intracavity field interference, the carrier dynamics can modify the cavity spectral response to the probe light. The population-inverted carriers modify the optical amplitude damping rate such that $\Gamma_p = \kappa/2 - \varphi(\Omega)\bar{N}$, effectively reducing the optical loss rate of the cavity and thus enhancing the radiation pressure [17]. For small probe signals, when $\bar{N}$ is below the laser threshold $N_{\text{th}} = \kappa/A_{21}$, the optical loss is partially compensated. However, when $\bar{N}$ is above the laser threshold, the optical damping rate becomes negative and the small probe signal will be amplified by the system. In what follows, we discuss the transmission of probe light in the below- and above-threshold regimes.

A. Below threshold

In this regime, the seeding signal serves as control light for the optomechanical coupling. First, we consider carrier population inversion below the laser threshold with $\bar{N} = 3 \times 10^5$. In a passive optomechanical system ($\bar{N} = 0$), the blue solid line in Fig. 3(b) shows the existence of a narrow transparency window for the probe light around the offset frequency $\Omega \approx \Omega_m$, where the probe light experiences an abrupt phase change, causing a large group delay. The delay time of slow light is associated with the optical damping rate. A smaller optical damping rate results in longer delay time. Figure 3(c) plots the delay time τ of the probe signal as a function of the optomechanical coupling strength.

In an active optomechanical system with $\bar{N} = 3 \times 10^5$, the cavity's effective optical damping rate $\Gamma_p/2\pi$ drops from 50 to ~21 MHz, leading to enhancement of radiation pressure. The red dashed line in Fig. 3(b) shows that the reduction of optical loss due to the carrier population inversion produces two effects: the cavity linewidth narrows and the probe field becomes undercoupled to the cavity. Meanwhile, the reduction of optical loss results in a larger phase change in the

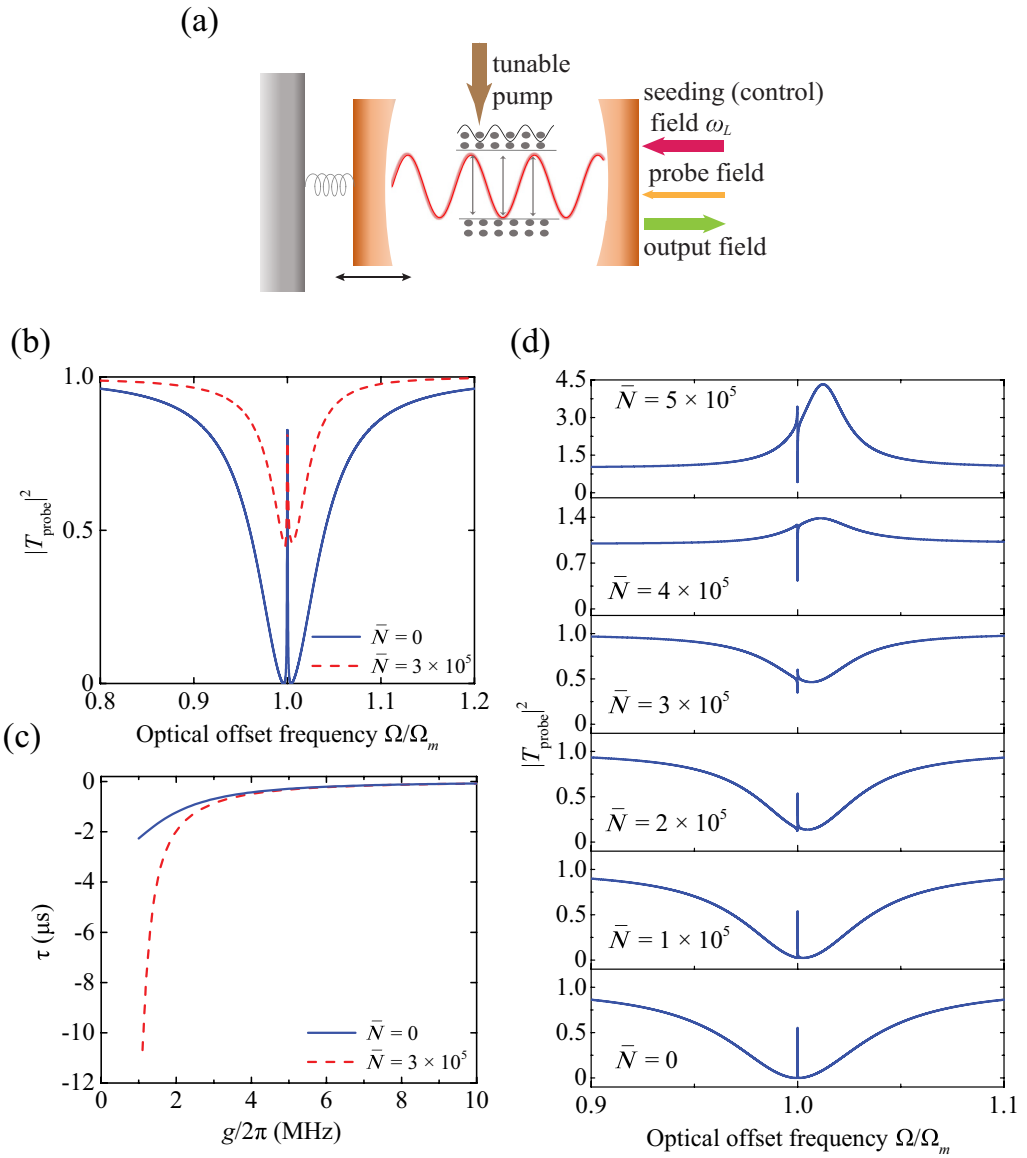

FIG. 3. (a) Schematic for exploring the carrier-induced gain effect in the semiconductor laser optomechanical system. While a seeding (control) field is coupled into the cavity to generate a lasing mode at frequency ω_L, an additional probe field is employed to measure the cavity transmission properties under different pump strength. (b) Transmission spectra of the probe field. The blue solid line plots the result for a passive optomechanical system where there is no carrier inversion ($\bar{N} = 0$). The red dashed line plots the result for an active optomechanical system where the inverted carrier population is $\bar{N} = 3 \times 10^5$. The optomechanical coupling rate $g/2\pi = Gx_{\text{ZPF}}\bar{n}^{1/2}/2\pi = 5$ MHz is assumed. (c) Group delay of the probe field for both a passive and an active optomechanical system operating below the threshold. (d) Transmission spectra of the probe field with increasing population of inverted carriers. The optomechanical coupling rate $g/2\pi = 1.2$ MHz is assumed. Parameters used in (b)–(d) are $(\Delta_{L\text{-cav}}/2\pi, \Delta_{L\text{-}a}/2\pi, \kappa/2\pi, T_p, T_N, \bar{n}, \mu_p, m_{\text{eff}}, \Gamma_m/2\pi, \eta_c) = (-1.25\,\text{GHz}, 1\,\text{GHz}, 100\,\text{MHz}, 16\,\text{ps}, 1.6\,\text{ns}, 2.5 \times 10^6, 1\,\text{MHz}, 1\,\text{ng}, 2 \times 10^4\,\text{Hz}, 0.5)$ [27,43].

transparency window, leading to a longer delay time. It is clear in Fig. 3(c) that with the same optomechanical coupling strength, the group delay τ in an active optomechanical system is significantly larger than that in a passive system.

B. Above threshold

Next, we focus on the above-threshold regime where the inverted carrier population $\bar{N}$ is greater than 4×10^5. Figure 3(d) plots the transmission spectra of the probe field with varying inverted carrier population. Below the laser threshold ($\bar{N} < 4 \times 10^5$), the transmission spectra exhibit the feature of OMIT, which is similar to that in passive optomechanical systems [10]. As the inverted carrier population increases beyond 4×10^5, the probe light can receive gain from the cavity, and thus the broad dip in the probe transmission spectra corresponding to the cavity resonance now becomes a broad peak. The peak transmission can be even

higher than that of the mechanically scattered sidebands. As a result, the phenomenon of OMIT now turns into OMIA. The line shape of the cavity response spectrum also depends on the inverted carrier population. As shown in Fig. 3(d), the transmission of the probe light near the mechanical resonant frequency changes from a Lorentzian to a Fano shape, as the inverted carrier population increases. The enhancement of inverted carrier population shifts the cavity resonance to a higher frequency and also changes the relaxation oscillation frequency, thus modifying the transmission line shape. Therefore, as an important degree of freedom, the introduced carrier population inversion can tune the transmission of probe light from OMIT to OMIA by increasing the inverted carrier population level.

In passive optomechanical systems [10,16,29–31], the probe light transmission properties such as delay time and transparency line shape can only be controlled with a coherent approach, e.g., by changing the strength of the control optical or electric field or varying detuning of the control light from the cavity resonance. Here, in an active optomechanical system, the probe light transmission properties can be controlled with an incoherent approach, by changing the inverted carrier population with an external pump which can be incoherent with the probe light. Such controlling flexibility features a unique advantage of active optomechanical systems compared with the conventional schemes.

V. CONCLUSION

We have investigated active cavity optomechanical systems where the cavity is constructed from an optical gain material. We have developed a comprehensive theoretical model to include the dynamics of optical field, mechanical mode, and inverted carrier population. We have analyzed two major effects introduced by the inverted carriers. First, the dynamics of carrier population leads to carrier relaxation oscillation, which is coupled dispersively to the intracavity optical field and consequently yields coherent coupling with the mechanical mode. This coupling mechanism can be employed to control the mechanical mode through a modulation to the pump. Second, the inverted carriers are also coupled dissipatively to the intracavity optical field because they can supply optical gain to compensate the loss of the cavity. Under this effect, the delay time of a probe light field can be tuned and largely enhanced, and it is also possible to tune the OMIT into OMIA.

Optomechanical systems have been employed as a versatile platform for conducting research in quantum physics and for developing quantum technologies [6,47,48]. This work has investigated the important role of an additional physical degree of freedom, i.e., inverted carriers, in conventional optomechanical systems, which opens a viable way to read out and control optomechanical interaction either coherently by coherent pump modulation (Sec. III) or incoherently by pump strength tuning (Sec. IV). On the other hand, optomechanical systems have also been employed for optical signal processing such as light storage and buffering via electromagnetically induced transparency [16,49] and OMIT [29]. Compared with their conventional counterparts, the laser optomechanical systems feature remarkably enhanced performance in light storage and buffering, and the optical delay time can also be tuned incoherently with greater flexibility (Sec. IV). In conclusion, the carrier-mediated cavity optomechanical systems in semiconductor lasers leverage inverted carriers, the new degree of freedom, to read out and control optomechanical interaction, enabling applications in mechanical state manipulation and light storage and buffering with flexible tunability in both coherent and incoherent fashions.

ACKNOWLEDGMENTS

This work was supported by the Early Career Scheme (Project No. 24208915) and the General Research Fund (Project No. 14208717) sponsored by the Research Grants Council of Hong Kong, and by the NSFC/RGC Joint Research Scheme (Project No. N_CUHK415/15) sponsored by the Research Grants Council of Hong Kong and the National Natural Science Foundation of China.

APPENDIX A: DERIVATION OF THE SUSCEPTIBILITY $\chi(\Omega)$

The laser dynamics is modeled by the interaction between matter and electromagnetic fields and described by the Lorenz-Haken equations. By including the optomechanical interaction term, the equations of motion for the optical field a, medium polarization p, and the inverted carrier population N are (in the rotating frame of laser frequency ω_L)

$$\dot{a} = \left(i\Delta_{L\text{-cav}} - \frac{\kappa}{2}\right)a - i\mu_p p + iGxa, \tag{A1}$$

$$\dot{p} = \left(i\Delta_{L\text{-}a} - \frac{1}{T_p}\right)p + i\mu_p aN, \tag{A2}$$

$$\dot{N} = \frac{1}{T_N}(N_{\text{st}} - N) + 2i\mu_p(a^* p - p^* a). \tag{A3}$$

Generally, the mechanical motion is modeled as

$$m_{\text{eff}}\left(\ddot{x} + \Gamma_m \dot{x} + \Omega_m^2 x\right) = \hbar G a^* a. \tag{A4}$$

In small-signal analysis for typical optomechanical systems, we can linearize the fields a, p, N, x by using the ansatz $a(t) = \bar{a} + \delta a(t)$, $p(t) = \bar{p} + \delta p(t)$, $N(t) = \bar{N} + \delta N(t)$, and $x(t) = \bar{x} + \delta x(t)$ since their fluctuations are much smaller than their steady-state values, and retain the first-order terms in the equations, yielding

$$\frac{d\delta a}{dt} = \left(i\bar{\Delta}_{L\text{-cav}} - \frac{\kappa}{2}\right)\delta a - i\mu_p \delta p + iG\bar{a}\delta x, \tag{A5}$$

$$\frac{d\delta p}{dt} = \left(i\Delta_{L\text{-}a} - \frac{1}{T_p}\right)\delta p + i\mu_p \delta(aN), \tag{A6}$$

$$\frac{d\delta N}{dt} = -\left(\frac{1}{T_N} + 2A_{21}\bar{n}\right)\delta N - 2A_{21}\bar{N}(\bar{a}\delta a^* + \bar{a}^*\delta a), \tag{A7}$$

$$m_{\text{eff}}\left(\frac{d^2\delta x}{dt^2} + \Gamma_m \frac{d\delta x}{dt} + \Omega_m^2 \delta x\right) = \hbar G(\bar{a}\delta a^* + \bar{a}^*\delta a), \tag{A8}$$

where $A_{21} = (2\mu_p^2/T_N)/(1/T_N^2 + \Delta_{L\text{-}a}^2)$ is the stimulated emission rate, and the approximation

$$p \approx \frac{i\mu_p a N}{i\Delta_{L\text{-}a} - 1/T_p} \tag{A9}$$

has been adopted in deriving Eq. (A7), which applies to typical lasers with $T_p \ll T_N$. If the laser's pump is perturbed by a small signal at frequency Ω, the inverted carrier population will carry a modulation term $\delta N_I = N_I \cos(\Omega t)$. Equations (A3) and (A7) are modified as

$$\dot{N} = \frac{1}{T_N}(N_{\text{st}} - N) + 2i\mu_p(a^* p - p^* a) + \delta N_I, \tag{A10a}$$

$$\frac{d\delta N}{dt} = -\left(\frac{1}{T_N} + 2A_{21}\bar{n}\right)\delta N - 2A_{21}\bar{N}(\bar{a}\delta a^* + \bar{a}^*\delta a) + \delta N_I. \tag{A10b}$$

To solve for the optical response to the drive modulation δN_I, we introduce the ansatz

$$\delta a(t) = A^- e^{-i\Omega t} + A^+ e^{i\Omega t}, \tag{A11a}$$

$$\delta p(t) = P^- e^{-i\Omega t} + P^+ e^{i\Omega t}, \tag{A11b}$$

$$\delta x(t) = X e^{-i\Omega t} + X^* e^{i\Omega t}, \tag{A11c}$$

$$\delta N(t) = N_0 e^{-i\Omega t} + N_0^* e^{i\Omega t} \tag{A11d}$$

into Eqs. (A5), (A6), (A8), and (A10b), then we obtain a set of coupled equations,

$$\left[-i(\bar{\Delta}_{L\text{-cav}} + \Omega) + \frac{\kappa}{2}\right]A^- = iG\bar{a}X - i\mu_p P^-, \tag{A12}$$

$$\left[-i(\bar{\Delta}_{L\text{-cav}} - \Omega) + \frac{\kappa}{2}\right]A^+ = iG\bar{a}X^* - i\mu_p P^+, \tag{A13}$$

$$\left[-i(\Delta_{L\text{-}a} + \Omega) + \frac{1}{T_p}\right]P^- = i\mu_p(\bar{a}N_0 + \bar{N}A^-), \tag{A14}$$

$$\left[-i(\Delta_{L\text{-}a} - \Omega) + \frac{1}{T_p}\right]P^+ = i\mu_p(\bar{a}N_0^* + \bar{N}A^+), \tag{A15}$$

$$(\Gamma_n - i\Omega)N_0 = -Q_0[A^- + (A^+)^*] + N_I, \tag{A16}$$

$$\Psi_m(\Omega)X = \hbar G\bar{a}[A^- + (A^+)^*], \tag{A17}$$

where

$$\begin{aligned} \Gamma_n &= \frac{1}{T_N} + 2A_{21}\bar{n}, \\ Q_0 &= 2A_{21}\bar{N}\bar{a}, \\ \Psi_m(\Omega) &= m_{\text{eff}}\left(-\Omega^2 - i\Gamma_m\Omega + \Omega_m^2\right). \end{aligned} \tag{A18}$$

If we introduce the definitions

$$\varphi(\Omega) = \frac{\mu_p^2}{-i(\Delta_{L\text{-}a} + \Omega) + 1/T_p}, \tag{A19}$$

$$f(\Omega) = -i(\bar{\Delta}_{L\text{-cav}} + \Omega) + \frac{\kappa}{2} - \varphi(\Omega)\bar{N}, \tag{A20}$$

and eliminate some terms in Eqs. (A12)–(A17), then we arrive at

$$f(\Omega)A^- = iG\bar{a}X + \varphi(\Omega)\bar{a}N_0, \tag{A21}$$

$$\left[\Gamma_n - i\Omega + \frac{\varphi^*(-\Omega)Q_0\bar{a}}{f^*(-\Omega)}\right]N_0 - \frac{iGQ_0\bar{a}}{f^*(-\Omega)}X = -Q_0A^- + N_I, \tag{A22}$$

$$\frac{\varphi^*(-\Omega)\hbar G\bar{n}}{f^*(-\Omega)}N_0 - \left[\Psi_m(\Omega) + \frac{i\hbar G^2\bar{n}}{f^*(-\Omega)}\right]X = -\hbar G\bar{a}A^-. \tag{A23}$$

By solving Eqs. (A21)–(A23), we obtain the expression of optical response to pump modulation,

$$A^- = \frac{\frac{\lambda(\Omega)\bar{a}[\varphi^*(-\Omega)+\varphi(\Omega)]}{f(\Omega)-f^*(-\Omega)} + \varphi(\Omega)\bar{a}}{\Omega_r^2 - \left(\Omega + \frac{\bar{\Delta}_{L\text{-cav}}}{2} + i\Gamma_r\right)^2 + (\Gamma_n - i\Omega)\lambda(\Omega)}N_I, \tag{A24a}$$

which is Eq. (5a) in the main text with

$$\lambda(\Omega) = \frac{i\hbar G^2\bar{n}[f(\Omega) - f^*(-\Omega)]}{f^*(-\Omega)\Psi_m(\Omega)}, \tag{A24b}$$

$$\Omega_r^2 = \frac{[\varphi^*(-\Omega)f(\Omega) + f^*(-\Omega)\varphi(\Omega)]Q_0\bar{a}}{f^*(-\Omega)} - \frac{(\Gamma_n - \Gamma_p')^2}{4}, \tag{A24c}$$

$$\Gamma_r = \frac{\Gamma_n + \Gamma_p}{2}, \tag{A24d}$$

$$\Gamma_p = \frac{\kappa}{2} - \varphi(\Omega)\bar{N}, \tag{A24e}$$

$$\Gamma_p' = -i\bar{\Delta}_{L\text{-cav}} + \frac{\kappa}{2} - \varphi(\Omega)\bar{N}. \tag{A24f}$$

APPENDIX B: DERIVATION OF THE TRANSMISSIVITY T_{probe} FOR THE PROBE SIGNAL

To study the response of a semiconductor laser optomechanical system to a weak probe field $E_p \exp[-i(\omega_L + \Omega)t]$, we conduct small-signal analysis where Eqs. (A5)–(A8) become (in the rotating frame of laser frequency ω_L)

$$\frac{d\delta a}{dt} = \left(i\bar{\Delta}_{L\text{-cav}} - \frac{\kappa}{2}\right)\delta a - i\mu_p\delta p + iG\bar{a}\delta x + S_{\text{in}}, \tag{B1a}$$

$$\frac{d\delta p}{dt} = \left(i\Delta_{L\text{-}a} - \frac{1}{T_p}\right)\delta p + i\mu_p\delta(aN), \tag{B1b}$$

$$\frac{d\delta N}{dt} = -\left(\frac{1}{T_N} + 2A_{21}\bar{n}\right)\delta N - 2A_{21}\bar{N}(\bar{a}\delta a^* + \bar{a}^*\delta a), \tag{B1c}$$

$$m_{\text{eff}}\left(\frac{d^2\delta x}{dt^2} + \Gamma_m\frac{d\delta x}{dt} + \Omega_m^2\delta x\right) = \hbar G(\bar{a}\delta a^* + \bar{a}^*\delta a), \tag{B1d}$$

where $S_{\text{in}} = \sqrt{\eta_c\kappa}E_p e^{-i\Omega t}$.

Introducing the same ansatz as that in Eq. (A11a)–(A11d), we obtain

$$f(\Omega)A^- = iG\bar{a}X + \varphi(\Omega)\bar{a}N_0 + \sqrt{\eta_c\kappa}E_p, \tag{B2a}$$

$$f(-\Omega)A^+ = iG\bar{a}X^* + \varphi(-\Omega)\bar{a}N_0^*, \tag{B2b}$$

$$(\Gamma_n - i\Omega)N_0 = -Q_0[A^- + (A^+)^*], \tag{B2c}$$

$$\Psi_m(\Omega)X = \hbar G\bar{a}[A^- + (A^+)^*]. \tag{B2d}$$

Using these four equations and eliminating A^+, N_0^*, and X^*, we obtain

$$f(\Omega)A^- = iG\bar{a}X + \varphi(\Omega)\bar{a}N_0 + \sqrt{\eta_c\kappa}E_p, \tag{B3}$$

$$\left[\Gamma_n - i\Omega + \frac{\varphi^*(-\Omega)Q_0\bar{a}}{f^*(-\Omega)}\right]N_0 + \frac{-iGQ_0\bar{a}}{f^*(-\Omega)}X = -Q_0A^-, \tag{B4}$$

$$\frac{-\varphi^*(-\Omega)\hbar G\bar{n}}{f^*(-\Omega)}N_0 + \left[\Psi_m(\Omega) + \frac{i\hbar G^2\bar{n}}{f^*(-\Omega)}\right]X = \hbar G\bar{a}A^-. \tag{B5}$$

Finally, we obtain the intracavity optical sideband A^- for the probe field E_p,

$$A^- = \frac{\left[(\Gamma_n - i\Omega) + \frac{\varphi^*(-\Omega)Q_0\bar{a}}{f^*(-\Omega)}\right] + (\Gamma_n - i\Omega)\frac{i\hbar G^2\bar{n}}{\Psi_m(\Omega)f^*(-\Omega)}}{\Omega_r^2 - \left(\Omega + \frac{\bar{\Delta}_{L\text{-cav}}}{2} + i\Gamma_r\right)^2 + (\Gamma_n - i\Omega)\frac{i\hbar G^2\bar{n}[f(\Omega) - f^*(-\Omega)]}{f^*(-\Omega)\Psi_m(\Omega)}}\sqrt{\eta_c\kappa}E_p. \tag{B6}$$

According to the input-output theory, the transmissivity of the probe light is expressed as

$$T_{\text{probe}} = \frac{E_p - \sqrt{\eta_c\kappa}A^-}{E_p} = 1 - \frac{\frac{\varphi^*(-\Omega)Q_0\bar{a}}{f^*(-\Omega)} + (\Gamma_n - i\Omega)\frac{f^*(-\Omega)\Psi_m(\Omega) + i\hbar G^2\bar{n}}{f^*(-\Omega)\Psi_m(\Omega)}}{\Omega_r^2 - \left(\Omega + \frac{\bar{\Delta}_{L\text{-cav}}}{2} + i\Gamma_r\right)^2 + (\Gamma_n - i\Omega)\lambda(\Omega)}\eta_c\kappa, \tag{B7}$$

which is Eq. (7) in the main text.

[1] M. Aspelmeyer, T. J. Kippenberg, and F. Marquardt, Rev. Mod. Phys. **86**, 1391 (2014).
[2] T. J. Kippenberg and K. J. Vahala, Science **321**, 1172 (2008).
[3] A. A. Clerk, M. H. Devoret, S. M. Girvin, F. Marquardt, and R. J. Schoelkopf, Rev. Mod. Phys. **82**, 1155 (2010).
[4] O. Arcizet, P. F. Cohadon, T. Briant, M. Pinard, and A. Heidmann, Nature (London) **444**, 71 (2006).
[5] S. Gigan *et al.*, Nature (London) **444**, 67 (2006).
[6] J. Chan, T. P. M. Alegre, A. H. Safavi-Naeini, J. T. Hill, A. Krause, S. Groblacher, M. Aspelmeyer, and O. Painter, Nature (London) **478**, 89 (2011).
[7] T. J. Kippenberg, H. Rokhsari, T. Carmon, A. Scherer, and K. J. Vahala, Phys. Rev. Lett. **95**, 033901 (2005).
[8] F. Marino, F. S. Cataliotti, A. Farsi, M. S. de Cumis, and F. Marin, Phys. Rev. Lett. **104**, 073601 (2010).
[9] A. H. Safavi-Naeini, S. Groblacher, J. T. Hill, J. Chan, M. Aspelmeyer, and O. Painter, Nature (London) **500**, 185 (2013).
[10] S. Weis, R. Rivière, S. Deléglise, E. Gavartin, O. Arcizet, A. Schliesser, and T. J. Kippenberg, Science **330**, 1520 (2010).
[11] D. Vitali, S. Gigan, A. Ferreira, H. R. Böhm, P. Tombesi, A. Guerreiro, V. Vedral, A. Zeilinger, and M. Aspelmeyer, Phys. Rev. Lett. **98**, 030405 (2007).
[12] Y.-D. Wang and A. A. Clerk, Phys. Rev. Lett. **110**, 253601 (2013).
[13] R. Ghobadi, S. Kumar, B. Pepper, D. Bouwmeester, A. I. Lvovsky, and C. Simon, Phys. Rev. Lett. **112**, 080503 (2014).
[14] E. Verhagen, S. Deleglise, S. Weis, A. Schliesser, and T. J. Kippenberg, Nature (London) **482**, 63 (2012).
[15] K. Y. Fong, L. Fan, L. Jiang, X. Han, and H. X. Tang, Phys. Rev. A **90**, 051801 (2014).
[16] A. H. Safavi-Naeini, T. P. M. Alegre, J. Chan, M. Eichenfield, M. Winger, Q. Lin, J. T. Hill, D. E. Chang, and O. Painter, Nature (London) **472**, 69 (2011).
[17] H. Ian, Z. R. Gong, Y.-x. Liu, C. P. Sun, and F. Nori, Phys. Rev. A **78**, 013824 (2008).
[18] A. Sanz-Mora, A. Eisfeld, S. Wüster, and J. M. Rost, Phys. Rev. A **93**, 023816 (2016).
[19] Y.-X. Huang, X.-F. Zhou, G.-C. Guo, and Y.-S. Zhang, Phys. Rev. A **92**, 013829 (2015).
[20] C. Genes, H. Ritsch, and D. Vitali, Phys. Rev. A **80**, 061803 (2009).
[21] M. J. Akram, M. M. Khan, and F. Saif, Phys. Rev. A **92**, 023846 (2015).
[22] M. Wallquist, K. Hammerer, P. Zoller, C. Genes, M. Ludwig, F. Marquardt, P. Treutlein, J. Ye, and H. J. Kimble, Phys. Rev. A **81**, 023816 (2010).
[23] S. Camerer, M. Korppi, A. Jöckel, D. Hunger, T. W. Hänsch, and P. Treutlein, Phys. Rev. Lett. **107**, 223001 (2011).
[24] K. Usami, A. Naesby, T. Bagci, B. Melholt Nielsen, J. Liu, S. Stobbe, P. Lodahl, and E. S. Polzik, Nat. Phys. **8**, 168 (2012).
[25] W. Yang, S. A. Gerke, K. W. Ng, Y. Rao, C. Chase, and C. J. Chang-Hasnain, Sci. Rep. **5**, 13700 (2015).
[26] F. Brennecke, S. Ritter, T. Donner, and T. Esslinger, Science **322**, 235 (2008).
[27] L. Ge, S. Faez, F. Marquardt, and H. E. Türeci, Phys. Rev. A **87**, 053839 (2013).

[28] C. Genes, D. Vitali, and P. Tombesi, Phys. Rev. A **77**, 050307 (2008).
[29] C. H. Dong, Z. Shen, C. L. Zou, Y. L. Zhang, W. Fu, and G. C. Guo, Nat. Commun. **6**, 6193 (2015).
[30] H. Wang, X. Gu, Y.-x. Liu, A. Miranowicz, and F. Nori, Phys. Rev. A **90**, 023817 (2014).
[31] J. Kim, M. C. Kuzyk, K. Han, H. Wang, and G. Bahl, Nat. Phys. **11**, 275 (2015).
[32] A. Jöckel, A. Faber, T. Kampschulte, M. Korppi, M. T. Rakher, and P. Treutlein, Nat. Nanotechnol. **10**, 55 (2014).
[33] X. Chen, Y.-C. Liu, P. Peng, Y. Zhi, and Y.-F. Xiao, Phys. Rev. A **92**, 033841 (2015).
[34] R.-P. Zeng, S. Zhang, C.-W. Wu, W. Wu, and P.-X. Chen, J. Opt. Soc. Am. B **32**, 2314 (2015).
[35] Y.-M. Liu, C.-H. Bai, D.-Y. Wang, T. Wang, M.-H. Zheng, H.-F. Wang, A.-D. Zhu, and S. Zhang, Opt. Express **26**, 6143 (2018).
[36] T. Li, S. Zhang, H.-L. Huang, F.-G. Li, X.-Q. Fu, X. Wang, and W.-S. Bao, J. Phys. B: At. Mol. Opt. Phys. **51**, 045503 (2018).
[37] C. Genes, H. Ritsch, M. Drewsen, and A. Dantan, Phys. Rev. A **84**, 051801 (2011).
[38] H. Yan, C. Jiong, and Z. Ling, J. Phys. B: At. Mol. Opt. Phys. **44**, 165505 (2011).
[39] Y. Xiao, Y.-F. Yu, and Z.-M. Zhang, Opt. Express **22**, 17979 (2014).
[40] K.-H. Gu, X.-B. Yan, Y. Zhang, C.-B. Fu, Y.-M. Liu, X. Wang, and J.-H. Wu, Opt. Commun. **338**, 569 (2015).
[41] L. Li, W. Nie, and A. Chen, Sci. Rep. **6**, 35090 (2016).
[42] G. P. Agrawal and N. K. Dutta, *Semiconductor Lasers*, 2nd ed. (Van Nostrand Reinhold, New York, 1993), Vol. 1.
[43] H. Haken, *Light: Laser Dynamics* (North-Holland, Amsterdam, 1985), Vol. 2.
[44] K. Vahala and A. Yariv, IEEE J. Quantum Electron. **19**, 1102 (1983).
[45] K. Vahala, C. Harder, and A. Yariv, Appl. Phys. Lett. **42**, 211 (1983).
[46] P. Meystre, E. M. Wright, J. D. McCullen, and E. Vignes, J. Opt. Soc. Am. B **2**, 1830 (1985).
[47] A. D. O'Connell *et al.*, Nature (London) **464**, 697 (2010).
[48] J. D. Teufel *et al.*, Nature (London) **475**, 359 (2011).
[49] M. Fleischhauer, A. Imamoglu, and J. P. Marangos, Rev. Mod. Phys. **77**, 633 (2005).